Trap-assisted transition between Schottky emission and Fowler-Nordheim tunneling in the interfacial-memristor based on Bi_2S_3 nano-networks

Ye Tian,[1,2,3,4,a] Lianjun Jiang,[1] Xuejun Zhang,[1] Guangfu Zhang,[1,2] and Qiuxiang Zhu[1]

[1]*School of Information and Electronics Engineering, Hunan City University, Yiyang 413000, China*
[2]*Hunan Province Higher Education Key Laboratory of Modeling and Monitoring on the Near-Earth Electromagnetic Environments, Changsha University of Science & Technology, Changsha 410000, China*
[3]*Photonic Research Group, Department of Information Technology, Ghent University-IMEC, Ghent B 9000, Belgium*
[4]*National Center for Nanoscience and Technology, China. No. 11, Beiyitiao, Zhongguancun 100190, China*

(Received 25 September 2017; accepted 12 February 2018; published online 5 March 2018)

For the usage of the memristors in functional circuits, a predictive physical model is of great importance. However, other than the developments of the memristive models accounting bulky effects, the achievements on simulating the interfacial memristance are still insufficient. Here we provide a physical model to describe the electrical switching of the memristive interface. It considers the trap-assisted transition between Schottky emission and Fowler-Nordheim tunneling, and successfully reproduces the memristive behaviors occurring on the interface between Bi_2S_3 nano-networks and F-doped SnO_2. Such success not only allows us uncover several features of the memristive interface including the distribution nature of the traps, barrier height/thickness and so on, but also provides a foundation from which we can quantitatively simulate the real interfacial memristor. https://doi.org/10.1063/1.5006433

I. INTRODUCTION

Memristance is an emerging new phenomenon occurring in nanoscale.[1] Electrically, it shows as that its resistance can be tuned by external voltage/current signal in a non-volatile manner,[1–3] and accordingly become a promising candidate for next-generation non-volatile memory featured with attractive speed, size, power consumption, and endurance.[2,4–7] Also, the memristive devices have already prompted remarkable interests and potentials in applications including intrinsic logic, neuromorphic computing, *etc*.[8–11] To further optimize the performance of the novel memristor and make progress in developing the circuits based on it, many studies were done over the last few years to reveal the mechanism of the memristor. At present, although there are still some issues in intensive debate, the physics picture about the generation of memristance are becoming increasingly clear. Take the oxide—the most important and representive family of memristive material—as an example, it is found that the mechanism of the oxide-based memristors could involve either the ion transport or electron transport processes.[12,13] Moreover, several analytical models accounting the effects of both ion transport and electron transport processes are proposed, and achieve great successes in capture important physical features of the memristor.[14] According to the prediction from analytical models as well as the experimental results of the real devices, the ion-transport-dominated devices

[a]Corresponding author. E-mail address: tianye-man@163.com.

seems with better retention performance, thus more valuable for the application like data storage. In contrast, for the purposes to electrically emulate the features of the synapse, or the behaviors of learning\memorizing, the electron-transport-dominated devices are still of significance,[11] since in these cases, the more critical property of the device is the continuous-tunability of the resistive state.

Recent years, in some chalcogenides, it was found that the electron trapping/detrapping process could produce memristive behaviors with satisfying continuous-tunability.[15] This is highly different from the conventional electrical switching of the chalcogenides based on crystalline/amorphous phase change produced by the current-induced Joule heat. Therefore more elaborations are needed to reveal the further details about such trap state in chalcogenides as well as its the influence to the memristive features. Very recently, the existence of scare oxygen within is proposed as the atomic origin to introduce traps in the sulfide—an important material group of the chalcogenides, providing us a valuable model system to understand the non-conventional memristive behaviors related to the traps in the chalcogenides.[16] A representive case of the memristor based on this concept is the interface between Bi_2S_3 nano-networks (BSNN) and F-doped SnO_2 (FTO), whose resistance state shows attractive bivariate-continuous-tunablity and similarity to the memorization of the brain.[3] In this system, the electrode is Schottky-contacted to the sulfides with traps, the co-impact of the Schottky barrier and the traps would produce the interface trap states.[17] Since the energy-level of the interface traps distributes continuously, the interfacial trapping/detrapping could tune the Schottky barrier and accordingly the resistive state of the interface continuously.[18] That is, the BSNN/FTO interface could behave exactly as a memristor. However, to quantitatively describe its memristive behaviors, it is needed to further reveal the variation of the electron conduction processes due to the interfacial trapping/detrapping. Moreover, considering the key to such memristance is proposed as the continuous distribution of the interfacial traps,[3] a reasonable description to the energy-level distribution of the traps is also of significance.

In this work, we take the aforementioned BSNN/FTO interface as the model system to explore the quantitative description to interfacial memristance on the basis of the understanding to the transition of the electron conduction processes during the memristive switching as well as the rational approaching to the distribution of interfacial traps. It founds that the trap-assitsed transition between Schottky emission (SE) and Fowler-Nordheim tunneling (FNT) occurs during the switching. A quantitative model considering such transition is constructed and used to simulate the memristive behaviors of the interface with (any) given trap-distribution. By comparing the memristive behaviors simulated under different trap-distribution, and fitting the model to I-V characteristics of the real BSNN/FTO device, we founds that the distribution of the interfacial traps is Gaussian-like. Due to the coexistence and competition of the influences of the Schottky barrier and the Fermi level pinning, the distribution of the interfacial traps is non-even broaden. The model presented in our investigations not only reflects the details of the switching dynamics but also is still simple enough to enable us to obtain valuable insight into the interfacial memristor based on carrier trapping/detrapping.

II. EXPERIMENTAL

A. Fabrication of the memristive interface

The start material to fabricate the BSNN is the amorphous BiO_x thin film, which is deposited on an FTO glass substrate by reactive sputtering (ULVAC, ACS-4000-C4). After deposition, the amorphous BiO_x thin film is annealed at 400 °C for 3 hours and then transform to β-Bi_2O_3. By immersing β-Bi_2O_3 film into a mixture of thioacetamide (TAA) and HCl at 60 °C for 72 hours, BSNN was achieved with thickness of 200 nm. When BSNN was sandwiched between Ag and FTO, the interfacial switchable device (Ag/BSNN/FTO) was produced. In this system, Ag is ohmic contacted to BSNN and the BSNN/FTO interface is with tunable Schottky barrier. The contact area of BSNN/FTO interface is a circle with diameter of 800 μm.

B. Characterizations and simulations

The morphology of BSNN was investigated by scanning electron microscopy (SEM, Hitachi S-4800). The memristance of BSNN/FTO interface are tested by a Keithley2635A sourcemeter. The simulation is carried out on Mathematica with self-programmed code.

III. RESULTS AND DISCUSSIONS

A. Physics picture of interface switching

Although the exact interfacial switching could be rather complicated and highly dependent on the material, fabrication method and/or condition, *etc.*,[3,11,18–20] briefly, we take BSNN/FTO interface as an example (Fig. 1a, the upper is the morphology of BSNN and the bottom is the configuration used to test the device based on BSNN/FTO interface),[3] ascribing the switching of the Schottky interface induced by trapping/detrapping processes as four stages shown in Fig. 1b: 1) In the Set stage, positive voltage is applied from Ag to FTO, thus the Schottky interface is reversely biased.[3,21] Generally, in this situation, for an ideal interface free of interfacial traps, few electrons move through the interface *via* Schottky emission process and only a low current could be observed.[17] However, if considerable traps exist in the interface and can capture the migrating electrons,[3,22] the electron-trapping would make the Schottky barrier lower and/or thinner.[6] Consequently, the interface conduction increases; 2) After the Set stage, the interface is switched to low resistive (LR) state with ohmic I-V characteristic. 3) Afterward, the negative voltage would release of the carriers from the traps, so the interface conduction decreases (Erase); 4) Finally, the interface is switched back from LR to high resistive (HR) state.

According to the physics picture of the interfacial switching given above, the critical process inducing the interface switching is the modulation of the Schottky barrier resulting from the electron trapping/detrapping. The further details, however, in the back of such modulation is not explicit. To figure out its nature in our BSNN/FTO interface, firstly, let us review all the possible electron conduction processes through the Schottky interface as shown in Fig. 2.[21,23] (1) Schottky emission: thermally activated electrons injected over the barrier into the conduction band; (2) Fowler-Nordheim (F-N) tunneling: electrons tunnel from the electrode into the conduction band, usually occurs at high field; If the interface has substantial number of traps (the distribution is schematically-illustrated by the blue line in Figure 2, and its details are discussed latter), trap-assisted-tunneling contributes to additional conduction, including the following steps: (3) tunneling from electrode to traps; (4) emission from trap to conduction band, which is essentially the Poole-Frenkel (P-F) emission; (5) F-N like tunneling from trap to conduction band. These electron conduction processes mentioned above, including Schottky emission, F-N tunneling and P-F emission, would produce different I-V behaviors:

For Schottky emission[3,17]

$$I = I_{SE} \exp(A\sqrt{V}) \tag{1}$$

where I_{SE} and A (>0) are two parameters related to Schottky emission behavior.

For F-N tunneling or FNT[17,21]

$$I = I_{FN} V^2 \exp(B/V) \tag{2}$$

where I_{FN} and B (<0) are two parameters related to F-N tunneling behavior.

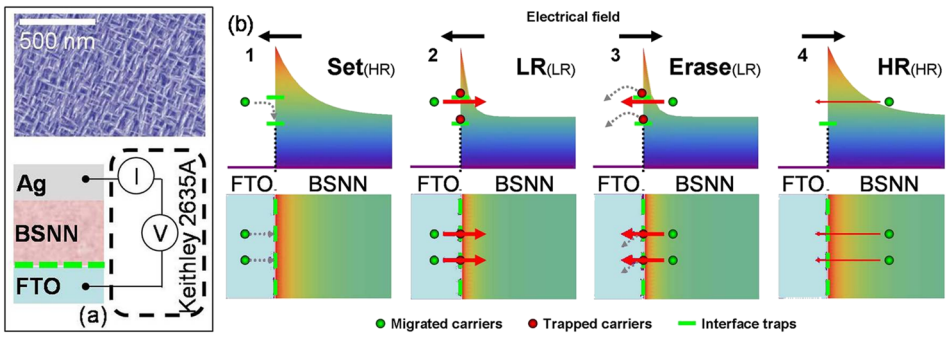

FIG. 1. (a) Morphology of BSNN and the configuration used to test the device based on BSNN/FTO interface; (b) Schematic illustration to the four stages of the switching of the memristive interface.

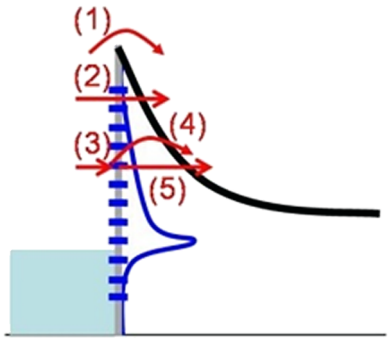

FIG. 2. Possible conduction mechanism in memristive interface: (1) Schottky emission; (2) Fowler-Nordheim (F-N) tunneling; (3) tunneling from electrode to traps; (4) emission from trap to conduction band; (5) F-N like tunneling from trap to conduction band.

For P-F emission[17,21]

$$I = I_{PF} V \exp(C\sqrt{V}) \tag{3}$$

where I_{FN} and C (>0) are two parameters related to P-F emission behavior. Such differences indicate that the mechanism of the interface switching is possible to be extracted *via* I-V fitting as discussed in the Section II B.

B. I-V behaviors and switching mechanism

Fig. 3a shows the measured bipolar switching behaviors of the BSNN/FTO interface. In the switching, there are clearly four consecutive stages: Set→Low resistive (LR)→Erase→High resistive (HR) under a voltage sweep (0 V→1V→-1V→0 V, the test configuration is shown Fig. 1a, in which the voltage bias is applied on Ag and the FTO is grounded). The most interesting feature we concern in the switching is that in the set stage, after the threshold voltage of V_{th}~0.25 V, the interface could be gradually switched to LR state (Note the switching inclination marked by dash line, distinguishing from the abrupt-jump of the resistance in regular resistive switching devices). Such tunability of the LR state is the most valuable property enables the BSNN/FTO interface work as a memristor and accordingly emulate the memorization of the brain.

To figure out the mechanism in the back of such memristive behavior, we replot the I-V curve at Set stage in the forms of ln$I$-*vs*-$V^{1/2}$, ln(I/V^2)-*vs*-V^{-1} and ln(I/V)-*vs*-$V^{1/2}$ to check their fitness to Schottky emission, F-N tunneling and P-F emission model, respectively. Fig. 3b shows that in the low

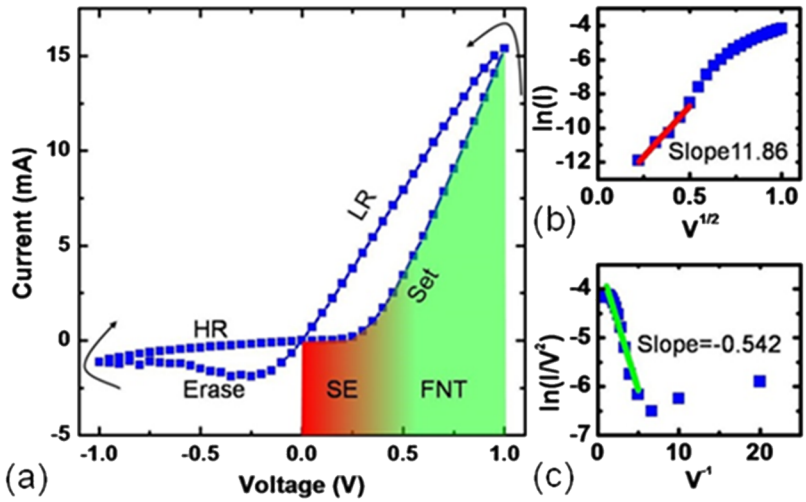

FIG. 3. (a) The measured I-V characteristics of the FTO/BSNN interface; (b) Schottky emission model fitting to data at low voltage range of Set stage; (c) Fowler-Nordheim tunneling model fitting to data at high voltage range of Set stage.

voltage range ($<V_{th}$) of the Set stage, the I-V follow the Schottky emission mechanism, while the F-N tunneling does not occur considering the slope of this range in $\ln(I/V^2)$-V^{-1} plot is positive. As the voltage increases ($>V_{th}$), the resistance of device gradually decrease, *i.e.*, it is set to LR state. In this range ($V_{th}\rightarrow 1V$), the experimental data deviate from Schottky emission mechanism, and become in line with F-N tunneling model (Fig. 3c). As for the P-F emission mechanism, it seems unreasonable because the linear-relationship was not observed in $\ln(I/V)$-$V^{1/2}$ plot (Sec. 1 of the supplementary material) over the whole Set stage in the range of both $0V\rightarrow V_{th}$ and $V_{th}\rightarrow 1V$. Therefore the continuous switching of the BSNN/FTO interfacial memristor in the SET stage from HR to LR should correspond to a variation of the electron conduction processes from Schottky-emission (SE, in the range $0V\rightarrow V_{th}$) to F-N tunneling (FNT, in the range $V_{th}\rightarrow 1V$) due to the occurrence of the electron-trapping. It is noteworthy that for the interface-controlled switching shown here, the tunneling is not through the whole BSNN layer (~200nm) but occur at the interface with a typical tunneling thickness of ~2.5nm (discussed latter). Besides, here other than the conventional tunneling model with the assumption of no trapping in interface or dielectric layer, the tunneling in our case should be still a trap-involved process, which is something like that observed in TiN/HfO_x/Pt system.[21] Therefore, here we name such variation as interfacial-trap-assisted SE-FNT transition. Obviously, this physics picture gives more details to the conduction mechanism of the memristor based on the BSNN/FTO interface in compare with our previous results where the investigations to the conduction process were mainly based on the analysis to the I-V curves in the range $0V\rightarrow V_{th}$.

The mechanism of the trap-assisted SE-FNT transition is also verified through ruling out some other candidates such as crystalline phase change, electrochemical switching based on Ag^+ motion, conducting filament formation/rupture process, space charge limited capture (the details about the exclusions of these mechanisms based on I-V analysis, energy-dispersive X-ray spectra and dark field transmission electron microscopy was discussed in Ref. 3). Additionally, in this study, the potential influences of serried resistor were avoided (note the test configuration shown in Figure 1a). Moreover, the existence of the rear oxygen at Bi_2S_3/FTO interface was revealed as the atomic origin of the traps very recently,[16] further supporting the rationality of the switching mechanism of the interfacial-trap-assisted SE-FNT transition.

C. Switching model

Different from the abrupt-jumped switching observed in other systems governed by the interfacial trapping/detrapping, here the BSNN/FTO interface shows continuous-tunable switching (memristance). This is because its interfacial trap states is not discrete but distribute continuously over a relative wide range. Therefore, below we consider the SE-FNT transition induced by capture/release of the carriers in interfacial traps with continuous distribution $g(E)$, and provide a quantitative description to the behaviors of the memristor based on the BSNN/FTO interface. As mentioned above, the bipolar-switching of BSNN/FTO interface contains four processes: 1) Set, 2) LR, 3) Erase and 4) HR. In the following, we discuss them in turn:

1. Set

In the set stage, the traps will be filled gradually. As a result, the memristor will transit from high resistive to low resistive. To quantitatively describe this gradual-varied process, we define $p_f(=N_f/N_t)$, which is the ratio of the filled traps N_f to all (fillable) traps N_t on the interface (at unit area). When a positive voltage V is applied and lasts for some time Δt, p_f will change to $p_f+\Delta p_f$ because of the trap-filling. Obviously, Δp_f (the variation of p_f during Δt) should be proportional to the number of the fillable traps below the energy level eV as well as the flux (or current) through them. The former term is

$$N_t\left(\frac{\int_{-\infty}^{eV} g(E)dE}{N_t} - p_f\right) \tag{4}$$

The latter one (current term) can be approximated by the Schottky emission current

$$I_{SE}\exp(A\sqrt{V}) \tag{5}$$

So

$$\frac{\Delta p_f}{\Delta t}(=\frac{dp_f}{dt}) \propto I_{SE}\exp(A\sqrt{V})N_t(\frac{\int_{-\infty}^{eV} g(E)dE}{N_t} - p_f) \tag{6}$$

If the time is long enough, all the fillable traps below the energy level eV would be filled, then

$$\frac{dp_f}{dt} \to 0, i.e., p_f(V) = \frac{\int_{-\infty}^{eV} g(E)dE}{N_t}, \tag{7}$$

Accordingly, on the interface, the current in the area with filled traps whose energy level is between E_F(=0 eV) and eV would follow the description of Eq. 2 (F-N tunneling), while the other area with un-filled traps is still with Schottky emission current. Consequently, the current on the device would be co-contributed by the current through the area with un-filled and filled traps as

$$\begin{aligned} I_{set} &= I_{SE}\exp(A\sqrt{V_{set}})N_t(1-p_f) + I_{FN}\exp(B/V_{set}){V_{set}}^2 N_t p_f \\ &= I_{SE}\exp(A\sqrt{V_{set}})[N_t - \int_{-\infty}^{eV_{set}} g(E)dE] + I_{FN}\exp(B/V_{set}){V_{set}}^2 \int_{-\infty}^{eV_{set}} g(E)dE \end{aligned} \tag{8}$$

2. LR

After set operation with voltage V_{set}, the device becomes low-resistive. Its conductance is

$$G_{set} = I_{set}/V_{set} \tag{9}$$

Thus at LR stage, the IV-characteristic is

$$I_{lr} = G_{set}V \tag{10}$$

3. Erase

Under the reversed electrical field, the release of the carriers filled in the traps would induce the closeness of the highly conductive current paths. The evolution of this process can be described by p_r, the ratio of the remained traps with releasable carriers to the number of total filled (thus releasable) traps after set operation with voltage V_{set}. The following factors are considered in describing its variation: On one hand, release should be proportional to the electrical field (or V) and remaining traps with releasable carriers ($N_t p_f\ p_r$). On the other hand, the faster the (reversed) electrical field is constructed, the quicker the carriers are released. Considering these factors, we obtain

$$-\frac{dp_r}{dt} \propto VN_t p_f p_r \frac{dV}{dt} \tag{11}$$

its solution is

$$p_r = \exp[-DN_t p_f(V_{set})V^2] \tag{12}$$

where D is a ratio parameter. As the carriers are released from the traps and the highly conductive current paths are closed, the transport behavior of the interface will gradually change from ohmic type to Schottky type. Therefore, in the Erase stage, the I-V characteristics are the superposition of ohmic and Schottky type transport:

$$I_{erase} = G_{set}p_r V + I_{SD}[1-\exp(-eV/nkT)](N_t - N_t p_f p_r) \tag{13}$$

where n is the ideality factor, k is Boltzmann's constant and T is the temperature.

4. HR

After the carriers in the traps are fully released, the I-V characteristics of the device are similar to a Schottky diode

$$I_{hr} = N_t I_{SD}[1-\exp(-eV/nkT)] \tag{14}$$

Combining the deduction shown above and choosing suitable units to make $N_t I_{SE}$=1, we can describe the I-V characteristics at the aforementioned four stages as following:

$$I_{Set} = \exp(A\sqrt{V})[1 - p_f(V)] + \frac{I_{FN}}{I_{SE}} \exp(B/V)V^2 p_f(V) \tag{15}$$

$$I_{LR} = G_{Set} V \tag{16}$$

$$I_{Erase} = G_{Set} p_r V + \frac{I_{SD}}{I_{SE}}[\exp(-eV/nkT) - 1][1 - p_f(V_{Set})p_r] \tag{17}$$

$$I_{HR} = \frac{I_{SD}}{I_{SE}}[\exp(-eV/nkT) - 1] \tag{18}$$

where $G_{Set} = I_{Set}/V_{Set}$ and $p_r = \exp[-D_t p_f(V_{Set})V^2]$ (here D_t=DN_t). And for the Schottky interface with traps (Sec. 2 of the supplementary material), *e.g.,* the FTO/BSNN system discussed here,

$$\frac{I_{SD}}{I_{SE}} \approx \exp(\frac{E_{ctr}}{2kT}) \tag{19}$$

where E_{ctr} denotes the weighting averaged energy level of all interface traps. On the other hand,

$$\frac{I_{FN}}{I_{SE}} = \frac{N_t d_t^2 e^3}{32R_0 T^2 h d^2 \Phi \exp[-\Phi/kT]} \tag{20}$$

where h is the plank constant, Φ is the barrier height, d is the averaged barrier thickness for F-N tunneling after electron trapping, R_0 (=1.20173×10^{6}A m^{-2}K^{-2}) is the Richardson constant, d_t is the typical size of the trap and the interface area (Sec. 2 of the supplementary material). Such that, given reasonable values to aforementioned parameters as well as the trap distribution, the whole four stages of the switching can be simulated.

To sum up, the model presented here endows a more clear physics picture to the LR-HR switching of the interfacial-trap-assisted SE-FNT transition comparing with our previous model.[3] Also in this improved model, the preset of special distribution of the traps is not required.[3] These advantages allowing us to extract more physical details about the memristance of BSNN/FTO interface as presented in following sections.

D. Trap distribution dependence of the switching

Considering our switching model shown above is suitable to any type of trap-distribution, we can simulate the switching behaviors at different distributions and compare them with the experimental results, so as to get the rational description to the interface traps distribution. In most cases, the traps distribution can be approached by either exponential or Gaussian function (the discrete trap can be regarded as the case of Gaussian distribution with zero-width). Hence below, we compare the simulated memristive behaviors of the interface with exponential- or Gaussian- distributed traps based on the switching model obtained in Section III C, and check which one is better to describe the distribution of the traps in BSNN/FTO interface.

In our previous works,[3] the distribution of the traps at the BSNN/FTO interface had be assumed as exponential:

$$D_{\exp}(E) = \frac{N_t}{E_t} \exp[-\frac{E_i - E}{E_t}] \tag{21}$$

where N_t the total concentration of electron traps, E_t the characteristic energy specifying the decay (width) of exponential-distribution, and E_i is the difference of the work function of FTO to that of Bi_2S_3. Using E_t =0.363 eV, and E_i =1.4 eV, we successfully produced the main features of the memristive behaviors observed in the BSNN/FTO interface.[3] Here we can further calculate for exponential-distribution

$$p_f(V) = \frac{\int_{-\infty}^{eV} D_{exp}(E)dE}{N_t} = \exp(-\frac{E_i - eV}{E_t}) = \exp(-\frac{1.4 - eV}{0.363}) \tag{22}$$

then the simulation based on the improved-model given above could well demonstrate the interfacial memristance as shown in Fig. 4a (solid blue line, see all parameters used for simulation in Sec. 3 of the supplementary material, and the solid red line corresponds to the experimental results for comparison). Likewise, we considering the switching behavior for the case of Gaussian distribution with N_t the total concentration of electron traps, σ_t the width of the distribution, and centered at E_{ctr}:

$$D_g = \frac{N_t}{\sqrt{2\pi}\sigma_t} \exp[-\frac{(E - E_{ctr})^2}{2\sigma_t^2}] \tag{23}$$

whose $P_f(V)$ can be similarly calculated as

$$P_f(V) = \frac{1}{2}[1 - Erf(\frac{E_{ctr} - eV}{\sqrt{2}\sigma_t})] \tag{24}$$

Then the switching behaviors of Gaussian case can be simulated as shown in Fig. 4b (solid black line, see all parameters used for simulation in Sec. 3 of the supplementary material, and the solid red line corresponds to the experimental results for comparison). Here the width (σ_t) is set as

$$\sigma_t = 4\sqrt{[E_t{}^2 - (kT)^2]/2\pi} (\approx 0.58eV) \tag{25}$$

This ensures the simulation to the Gaussian case well-comparable with the aforementioned exponential case as presented in Nicolai, H. *et. al.* 's work.[24] While the E_{ctr} at the interface, considering the pining of the Femi level,[25] is suggested to be close to that in BSNN itself (~0.317 eV, extracted from the connection between Meyer-Neldel relationship and photocurrent decay of BSNN[26]). Comparing Fig. 4a and 4b, it founds that the switching of the exponential-distributed traps is steady (dash blue line in Fig. 4a), while for the Gaussian-distributed traps, the switching is more moderate (dash black line in Fig. 4b) and relatively closer to experimental results of the FTO/BSNN system (Note the dash red line in both Fig. 4a and 4b). Therefore, we argue that the traps distribution at FTO/BSNN interface is Gaussian-like.

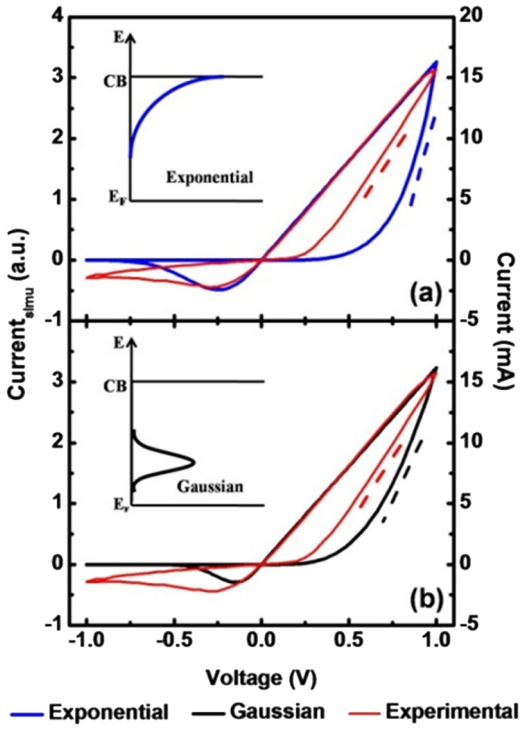

FIG. 4. Comparison between experimental results and the simulated I-V curve using (a) exponential-distributed traps, and (b) Gaussian-distributed traps.

In fact, it is not surprise that the distribution of the traps inducing the interfacial memristance is not exponential- but Gaussian-like, considering the main part of the exponential-distributed traps is close to the conductance band bottom (shadow traps) as shown in the inset of the Fig. 4a and accordingly cannot trap the electrons stably. Whereas for the Gaussian-case, most traps are deep ones (relative closer to Femi level, see the inset of the Fig. 4b), which is much more beneficial to produce robust switching.

E. Model-fitting to experimental I-V characteristics

Although the studies given in Section III D show that the traps inducing switching should be Gaussian-distributed, the simulated I-V characteristics still do not perfectly reproduce the experimental behaviors (Fig. 4b). This is because the distribution parameters used in the simulation is obtained from the assumed exponential-distribution (see Eq. 25), which does not accurately reflect the distribution feature of the traps. To further reveal the exact distribution nature of the interface traps, we fit the experimental I-V curve with our switching model (Sec. 4 of the supplementary material).

As shown in Fig. 5, good fitness is obtained at all the four stages (Set, LR, Erase and HR) with the parameters listed in Table I, including successfully reproduce the moderated switching in Set stage as well as the negative differential resistance appearing in Erase stage. The fitted I-V curves indicate that the Gaussian-distributed interface traps are centered at 0.317 eV with "width" σ_t of 0.253 eV. Comparing with the traps in BSNN itself (E_t~0.317 eV, σ_t~0.055 eV, extracted from the connection between Meyer-Neldel relationship and photocurrent decay of BSNN[26]), the distribution

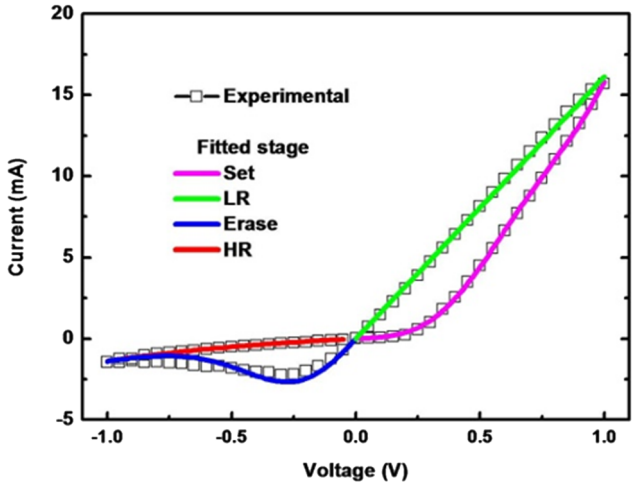

FIG. 5. Model-Fitting to the four stages of the switching on BSNN/FTO interface.

TABLE I. Parameters for model-fitting to I-V characteristics of BSNN/FTO interface.

Parameter	Fitting Value
E_{ctr}	0.317 eV
σ_t	0.253 eV
T	293 K
A	11.86
B	-0.542
$N_t I_{SE}$	2.726×10^{-3} mA
$N_t I_{FN}$	24.9 mA/V^2
G_{set}	16.12 mS
D_t	7.292
$N_t I_{SD}$	0.6765 mA
nkT	0.9 eV

is remarkably broaden because of the effects of the Schottky barrier (but it should be emphasized that such broaden is not even, which will be discussed in Section III F).

Besides the distribution nature, some other interfacial features can be also obtained from the fitted results:

1) Note I_{SD}/I_{SE}=248.2, then E_{ctr} can be determined by Eq.19 as 0.287 eV, which is close to that recently extracted from the connection between Meyer-Neldel relationship and photocurrent decay of BSNN (~0.317 eV).[26]
2) The SE-FNT transition occurs as the voltage>V_{th} (see Fig. 3a), and on the other hand, it is known that the F-N tunneling usually begins to make apparent contribution to the current as the electric field strengths is higher than 10^8 V m^{-1}.[27] So the barrier thickness of the F-N tunneling (d) can be estimated as 2.5 nm (=$V_{th}/10^8$ V m^{-1}), accounting well with the results of Zhong-Tang Xu *et. al.* and Shimeng Yu *et. al.*[6,21] Furthermore, assuming the trap concentration in BSNN is ~$10^{14}$$cm^{-3}$ (Sec. 5 of the supplementary material), we can estimate N_t~1×$10^{14}$$cm^{-3}$×$d$=2.5×$10^7$$cm^{-2}$. If note recently the origin of the trap is suggested as the existence of the residual oxygen in BSNN,[22,28] the size of the trap (d_t) can be deemed as the diameter of the O-atom in Bi_2S_3 (~0.4 nm). Hence considering I_{FN}/I_{SE}=9120.88, and substitute the value of the parameters given above into Eq. 20, we can get barrier height Φ=0.653 eV. Comparing with the barrier height predicted by the traditional Schottky-Mott rule (0.873 eV, Sec. 6 of the supplementary material),[17] Φ determined by model-fitting is smaller. This should be attributed to the impact of the interfacial traps. Exactly, here the SE-FNT transition occurring in memristive interface is a trap-assisted process. That is, the tunneling is not directly from electrode to the conduction band, but intermediated with the traps.[21] Hence the effective barrier height for tunneling is lower because of the fact that the energy levels of the electron traps are higher that the Fermi level (Fig. 2). The difference of the barrier-height value (0.22 eV) is account with the critical voltage of the SE-FNT transition (V_{th}~0.25 V), further supporting such explanation to the smaller barrier-height.

F. Coexistence and competition of Schottky barrier and Fermi level pinning

As mentioned above, the broaden of the trap-distribution due to the influences of the Schottky barrier is not even: the extracted "width" σ_t of 0.253 eV is more reasonable to be deemed as an average of the broaden effect. This is induced by the coexistence and competition of the influences of the Schottky barrier and Fermi level pinning as discussed below.[22]

Exactly, due to the influences of the Schottky barrier, the conductance band bottom of BSNN near the interface would be bent.[17] Accordingly, along with the variation of the conductance band bottom, the shallow traps become higher. Such effect induces the broaden of the distribution of the trap level at high energy range.[17,22] Whereas the deep traps are far away from the conductance band bottom, and thus almost not affected by the bending of the conductance band.[17,22] Hence they remain on their own energy levels as in the bulky statues due to the pinning of the Fermi level.[25] Consequently, a more rational distribution of the traps in the BSNN/FTO interface is something like that shows in Fig. 6 (or blue line of Fig. 2), which was semi-quantitatively extracted using the method proposed in our previous work based on the comparison between photocurrent decay of BSNN and the I-V characteristics of BSNN/FTO interface.[22] To further understand such non-even broaden owing to the coexistence and competition of the influences of Schottky barrier and Fermi level pinning, we use the Gaussian function to match the different range of this semi-quantitative trap distribution D(E).

Obviously, although the most part of the conduction is from the trap-involved-process, the influences of some other factors still exist, and their impacts is not subtracted in the photocurrent and/or I-V characteristics used to analysis the profile of the trap distribution.[22] Hence to provide a more rational Gaussian-matching to this profile, the function below is used

$$y = a\exp[-\frac{(E-\mu)^2}{2\sigma^2}] + b \tag{26}$$

In this function, a and b are two parameters respectively reflecting the proportion of Gaussian (trap-involved-process) and non-Gaussian part (others), μ is fixed as E_{ctr}(=0.317 eV), and σ is set as 0.055 eV, 0.165 eV, 0.253 eV and 0.51 eV respectively, to match the different ranges of the profile

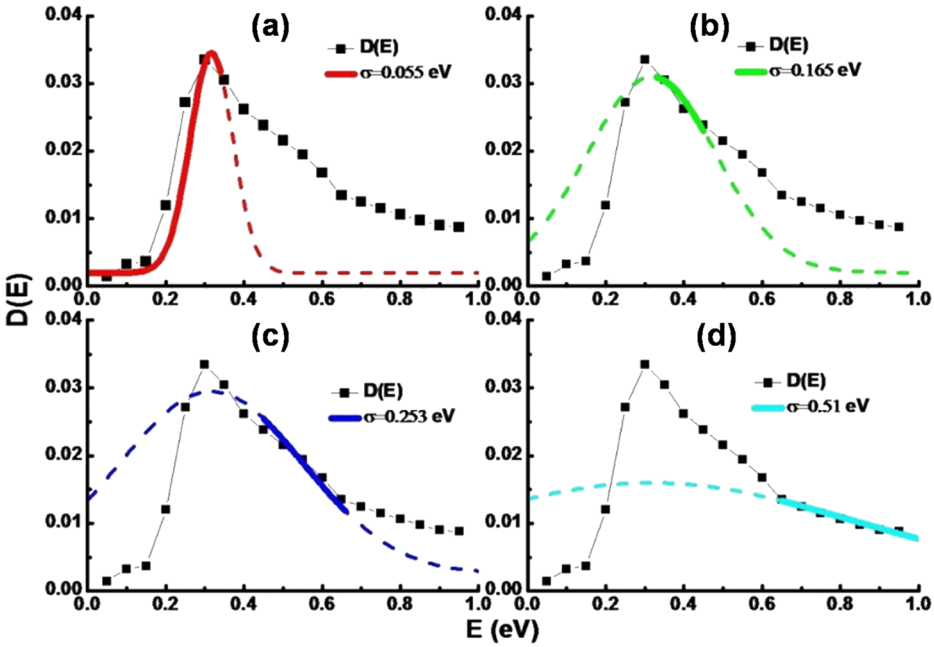

FIG. 6. The energy-level-distribution of the interfacial traps (D(E), extracted from the comparison between photocurrent decay of BSNN and the I-V characteristics of BSNN/FTO interface, see Ref. 22, (reproduced with permission from Tian *et al.* Nanoscale **8**(2), 915–920 (2016). Copyright 2016 The Royal Society of Chemistry) matched by Gaussian function centered at 0.317 eV but with different width: (a) σ_t=0.055eV; (b) σ_t=0.165eV; (c) σ_t=0.253eV; (d) σ_t=0.51eV (dash lines in figures are for guiding the eyes-view).

TABLE II. Parameters for Gaussian-matching to this trap-distribution at BSNN/FTO interface.

No.	μ/eV	σ/eV	*a*	*b*
1	0.317	0.055	0.0325	0.002
2		0.165	0.0305	
3		0.253	0.0270	
4		0.510	0.0140	

which is Gaussian-like but non-even broaden. Four Gaussian functions used for matching are listed in Table II and shown in Fig. 6a–6d. It is clearly to see that *a* is always much larger than *b*, confirming the dominated role of the trap-involved process in BSNN/FTO interface. Moreover, we found that the broaden in the range close to Fermi level is rather slight, and become increasingly apparent as the energy level rise up (Fig. 6a–6d), agreeing well with the expected non-even broaden of the trap distribution due to aforementioned coexistence and competition of the influences of Schottky barrier and Fermi level pinning. Additionally, it can be picked out that the larger the σ, the smaller the *a* (Table II). If note *a* is proportional to the trap number (easily found from comparing with Eq.23), such feature would indicate that along with the larger broaden of the trap-distribution as the energy level rise up, the number of the traps being broaden decreases. This is also tolerant with the fact that the interfacial traps is Gaussian but not exponential.

IV. CONCLUSION

In summary, we proposed an interfacial memristance model and fitted it to our experimental measurement data of the Ag/BSNN/FTO memristor devices. The model considers the interfacial-trap-assisted transition between the Schottky emission and the Fowler-Nordheim tunneling, and accounts the continuous distribution of the interfacial traps. It reproduced the experimental data

accurately, including the gradual switching from high resistive to low resistive state, as well as the negative differential conductance feature in the erase-stage. From the model-fitting, several properties of the memristive interface were extracted such as the barrier height, center and width of the trap distribution, and so on. The model presented here could be a foundation for performing more complete simulations to interfacial memristor.

SUPPLEMENTARY MATERIAL

See supplementary material for further discussions about the fitness to P-F emission model, pre-factors in the switching model, parameters used for simulation, the procedure of model-fitting, trap concentration in interface and the barrier height of the interface with traps.

ACKNOWLEDGMENTS

This research was supported by NSFC (11547163, 11604091, 1547186), the Hunan provincial natural science foundation (2015JJ6015), the Open Research Fund of the Hunan Province Higher Education Key Laboratory of Modeling and Monitoring on the Near-Earth Electromagnetic Environments, Changsha University of Science & Technology, and the research foundation of education bureau of Hunan province, China (16B048). Ye Tian thanks for the fellowship from the China Scholarship Council (CSC, No. 201508430266).

[1] D. B. Strukov, G. S. Snider, D. R. Stewart, and R. S. Williams, Nature **453**(7191), 80–83 (2008).
[2] B. Sun, W. Zhao, Y. Liu, and P. Chen, Functional Materials Letters **8**(01), 1550010 (2015).
[3] Y. Tian, C. Guo, S. Guo, T. Yu, and Q. Liu, Nano Research **7**(7), 953–962 (2014).
[4] Q. Liu, W. Guan, S. Long, R. Jia, M. Liu, and J. Chen, Applied Physics Letters **92**(1), 12117 (2008).
[5] W. Lu and C. M. Lieber, Nature Materials **6**(11), 841–850 (2007).
[6] Z. T. Xu, K. J. Jin, L. Gu, Y. l. Jin, C. Ge, C. Wang, H. Z. Guo, H. B. Lu, R. Q. Zhao, and G. Z. Yang, Small **8**(8), 1279–1284 (2012).
[7] J. J. Yang, M. D. Pickett, X. Li, D. A. Ohlberg, D. R. Stewart, and R. S. Williams, Nature Nanotechnology **3**(7), 429–433 (2008).
[8] S. H. Jo, T. Chang, I. Ebong, B. B. Bhadviya, P. Mazumder, and W. Lu, Nano Letters **10**(4), 1297–1301 (2010).
[9] S. Kvatinsky, G. Satat, N. Wald, E. G. Friedman, A. Kolodny, and U. C. Weiser, IEEE Transactions on Very Large Scale Integration (VLSI) Systems **22**(10), 2054–2066 (2014).
[10] J. Borghetti, G. S. Snider, P. J. Kuekes, J. J. Yang, D. R. Stewart, and R. S. Williams, Nature **464**(7290), 873–876 (2010).
[11] R. Pan, J. Li, F. Zhuge, L. Zhu, L. Liang, H. Zhang, J. Gao, H. Cao, B. Fu, and K. Li, Applied Physics Letters **108**(1), 013504 (2016).
[12] K. Kyung Min, J. Doo Seok, and H. Cheol Seong, Nanotechnology **22**(25), 254002 (2011).
[13] G. Ella, Semiconductor Science and Technology **29**(10), 104004 (2014).
[14] D. B. Strukov, J. L. Borghetti, and R. S. Williams, Small **5**(9), 1058–1063 (2009).
[15] Y. Li, Y. Zhong, L. Xu, J. Zhang, X. Xu, H. Sun, and X. Miao, Scientific Reports **3**, 1619 (2013).
[16] Y. Tian, L. Pan, C. F. Guo, and Q. Liu, Nano Research **10**(6), 1924–1931 (2017).
[17] M. A. Lampert and P. Mark, *Current injection in solids* (Academic Press, 1970).
[18] A. Sawa, Materials Today **11**(6), 28–36 (2008).
[19] R. Waser, R. Dittmann, G. Staikov, and K. Szot, Advanced Materials **21**(25-26), 2632–2663 (2009).
[20] J. J. Yang, D. B. Strukov, and D. R. Stewart, Nat Nano **8**(1), 13–24 (2013).
[21] S. Yu, X. Guan, and H.-S. P. Wong, Applied Physics Letters **99**(6), 063507 (2011).
[22] Y. Tian, J. Zhang, C. F. Guo, B. Zhang, and Q. Liu, Nanoscale **8**(2), 915–920 (2016).
[23] G. Jegert, A. Kersch, W. Weinreich, U. Schröder, and P. Lugli, Applied Physics Letters **96**(6), 062113 (2010).
[24] H. Nicolai, M. Mandoc, and P. Blom, Physical Review B **83**(19), 195204 (2011).
[25] F. Léonard and J. Tersoff, Physical Review Letters **84**(20), 4693 (2000).
[26] Y. Tian, L. Jiang, X. Zhang, and G. Zhang, Journal of Physics D: Applied Physics **49**(40), 405107 (2016).
[27] E. L. Murphy and R. H. Good, Physical Review **102**(6), 1464–1473 (1956).
[28] Y. Tian, C. F. Guo, J. Zhang, and Q. Liu, Physical Chemistry Chemical Physics **17**(2), 851–857 (2015).